hydrogen

MDPI

Article

A One-Dimensional Computational Model to Identify Operating Conditions and Cathode Flow Channel Dimensions for a Proton Exchange Membrane Fuel Cell

Nikolaj Maack Bielefeld, Rasmus Dockweiler Sørensen, Mikkel Jørgensen, Kristoffer Kure and Torsten Berning *

AAU Energy, Aalborg University, DK-9220 Aalborg, Denmark
* Correspondence: tbe@energy.aau.dk

Abstract: A one-dimensional computational model has been developed that can be used to identify operating conditions for the cathode side of a proton exchange membrane fuel cell such that both the inlet and outlet relative humidity is equal to 100%. By balancing the calculated pressure drop along the cathode side flow channel with the change in molar composition, inlet conditions for the cathode side can be identified with the goal of avoiding channel flooding. The channel length, height, width and the land-to-channel width ratio are input parameters for the model so that it might be used to dimension the cathode flow field. The model can be used to calculate the limiting current density, and we are presenting unprecedented high values as a result of the high pressure drop along the flow channels. Such high current densities can ultimately result in a fuel cell power density beyond the typical value of 1.0–2.0 W/cm^2 for automotive fuel cells.

Keywords: proton exchange membrane fuel cell (PEMFC); operating conditions; flow field design; pressure drop; high current density; porous metal plates

check for updates

Citation: Bielefeld, N.M.; Sørensen, R.D.; Jørgensen, M.; Kure, K.; Berning, T. A One-Dimensional Computational Model to Identify Operating Conditions and Cathode Flow Channel Dimensions for a Proton Exchange Membrane Fuel Cell. *Hydrogen* **2024**, *5*, 624–643. https://doi.org/10.3390/hydrogen5030033

Received: 6 August 2024
Revised: 3 September 2024
Accepted: 5 September 2024
Published: 10 September 2024

1. Introduction

As proton exchange membrane fuel cells (PEMFCs) are becoming wider spread and accepted, there is a general requirement to further increase the power density, especially if new, high power density applications such as airplanes should become a reality. Currently, the volumetric power density of a liquid-cooled fuel cell stack by Ballard Power Systems is 4.3 kW/L excluding endplates [1]. A schematic of a PEMFC is shown in Figure 1.

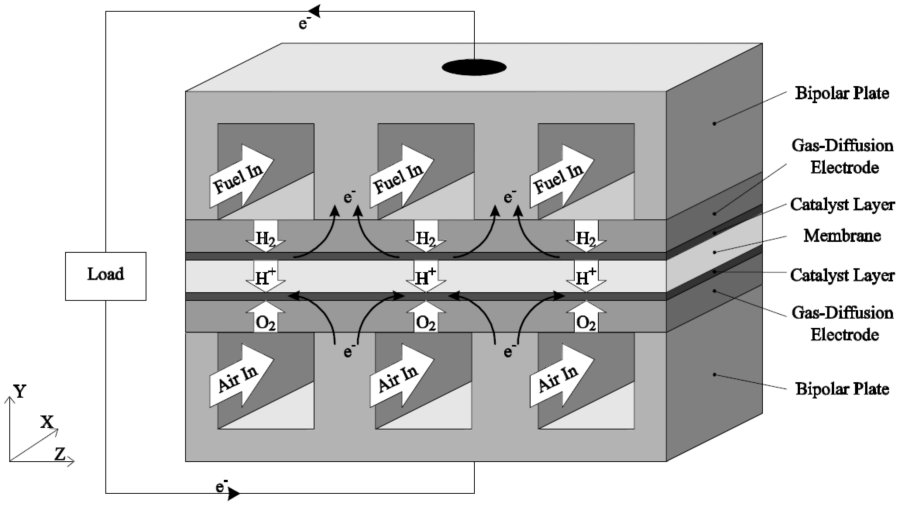

Figure 1. PEMFC schematic [2]. Upper part is anode and lower part cathode.

In PEMFCs, hydrogen is internally combined with oxygen from air to create water and generate electricity according to the following reactions:

Anode:

$$2H_2 \Rightarrow 4H^+ + 4e^- \quad (1)$$

Cathode:

$$O_2 + 4H^+ + 4e^- \Rightarrow 2H_2O \quad (2)$$

Combined:

$$2H_2 + O_2 \Rightarrow 2H_2O \quad (3)$$

The molar amount of the consumed oxygen and hydrogen is related to the generated electricity via Faraday's law:

$$\dot{n}_{H_2,cons.} = \frac{I}{2F} \quad (4)$$

and

$$\dot{n}_{O_2,cons.} = \frac{I}{4F} \quad (5)$$

where F is Faraday's constant (96,485 C/moles) and I is the total current generated, i.e., the current density in every cell multiplied with the area of the cell and the number of cells in a fuel cell stack that can be 200 and more in automotive applications.

Figure 2 shows a common fuel cell performance and power curve and the main losses. It is quite typical that the power density of the fuel cell peaks at 80% of the maximum, limiting current density. In fuel cell textbooks this limiting current density is usually between 1.0 and 2.0 A/cm^2, but automotive fuel cell manufacturers have probably surpassed these values.

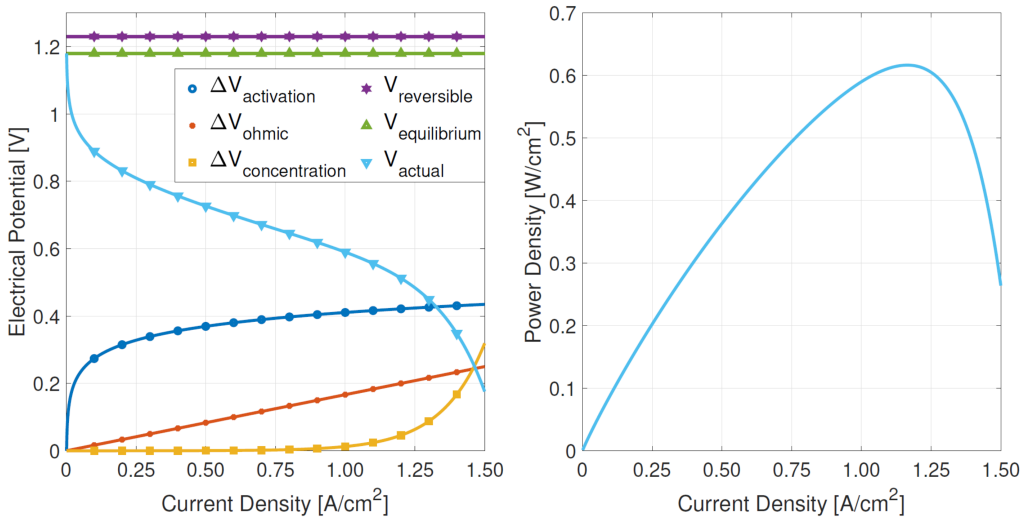

Figure 2. Typical PEMFC performance curve and main loss mechanisms.

The cell voltage of a single cell begins at the theoretical maximum of 1.23 V as dictated by the Nernst equation. As the current density increases, there is a steep decline in fuel cell voltage owing to the activation overpotentials that can be calculated with the Butler-Volmer equation or by the Tafel equation. Further increasing the current density, there is a linear drop-off in cell potential owing to an ohmic type of resistance, mainly caused by losses in the polymer electrolyte membrane and by contact resistances [3]. Finally, the performance typically decreases steeply as mass transport limitations set in. The area power density of fuel cells is the product of the cell voltage and the current density. For automotive fuel cells, a target value of 1.0 W/cm^2 has been proclaimed by the Department of Energy (DOE) and has been reached by automotive manufacturers.

Owing to mass transport limitations, both the air and the hydrogen enter at a flow rate higher than is dictated by Faraday's law. The stoichiometric flow ratio, here denoted λ, is defined as the molar flow rate of reactants entering the fuel cell over the molar amount of reactants that are consumed in the electrochemical reactions, e.g., for the cathode side:

$$\dot{n}_{O_2,in} = \lambda_c \times \dot{n}_{O_2,cons.} \quad (6)$$

Because the cathode side in a fuel cell is usually operated on air, the amount of air that is fed to the stack is accordingly higher. In general, the compressor work to supply the air is among the highest parasitic power consumers in a fuel cell system, and therefore the stoichiometry should be kept low (e.g., [4,5]). In a PEM fuel cell, the maximum current density is limited by two physical effects:

- Mass transport limitations owing to the limited diffusion of oxygen to the reaction sites. The equation that permits the calculation of this limiting current density for a straight channel flow field will be shown below, and it is a direct function of the oxygen concentration in the gas flow channels [5]. However, this equation includes only the diffusive transport from the flow channels towards the catalyst layer, but not the dissolution of oxygen into the electrolyte phase.
- Membrane overheating and a strong increase in cell temperature with increasing current density. Both experiments [6,7] and simulations [8–10] have shown that the temperature can rise as much as 10 °C at high current densities at the catalyst layer and the membrane. While a higher temperature generally enhances the electrochemical reactions, it was found that the proton conductivity of Nafion membranes is at a peak at 60–70 °C, and it decreases steeply as the temperature increases beyond 75 °C [11,12].

To increase the current density beyond conventional values, both of these issues must be resolved. The latter issue of overheating is closely related to the thermal conductivity of the commonly employed porous gas diffusion layers (GDL) [9] which are in the region of 0.5 W/mK [13], and which increases to values between 1–2 W/mK when liquid water is present under wet operating conditions [14]. The values for the dry thermal conductivities were also obtained with a model by Yablecki and Bazylak [15].

The effect of GDL with varying thermal conductivity on the fuel cell performance was recently investigated by Csoklich et al. [16], who concluded that thermal conductivity should not be a decisive criterion for future materials developments of optimized GDLs to improve fuel cell performance at high current densities, but rather the GDL structure. The artificially made porous transport layer with the lowest thermal conductivity exhibited the best cell performance and the highest limiting current density. However, a two-dimensional modeling study in that work also revealed that the membrane temperature for the case showing the best performance was as high as 95 °C for the same heating terms, although the nominal cell operating temperature was 80 °C in all cases, and it is therefore doubtful whether the current density can be further increased beyond values of 1.5–2.0 A/cm^2.

Fernihough et al. studied the effect of PEMFC operating at temperatures as high as 120 °C using Nafion 212 membranes, and they found maximum current densites in the region of 1.5 A/cm^2 at 80 °C which increased to 1.8 A/cm^2 at 100 °C, but decreased to only around 1.2 A/cm^2 at 120 °C [17].

In recent years, there have been efforts to replace the expensive carbon fibre papers (CFPs) by cheaper perforated metal plates. With a thickness in the order of 50 microns, these plates are also thinner than typical CFP [18]. To allow for under-land diffusion, these metal GDLs need to be combined with a stand-alone micro-porous layer (MPL) which is typically in the order of 50 microns thick [18], see Figure 3 below. The holes in the metal plates are created with a chemical edging process, and they are 60–120 microns, whereas the typical pore size of CFP is in the order of 10–50 microns [19], and while CFP have porosities of 80–90%, the porosity of these metal plates is around 30–40%. Hussein et al. have studied the performance of PEMFC with perforated metal plates, and the results were very encouraging [18]. Compared to a fuel cell with a Freudenberg H2315 GDL, the

cells with a perforated metal GDL showed an increased limiting current density of around 2 A/cm^2, and an improved performance, partly owing to a decreased ohmic resistance.

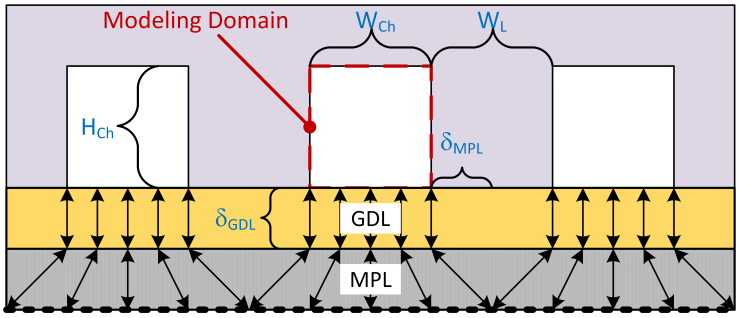

Figure 3. The modeling domain includes only one flow channel and information about the channel and land width.

Tanaka and Malan employed the computational fluid dynamics (CFD) software STAR-CCM+ 12.02 (SiemensPLM, Plano, TX, USA) to study the performance of such metal plates with honeycomb holes [20]. The model included detailed electrochemistry, and they found a suggested improvement of 9.4% in cell power density. This model was single phase and did not include a prediction of the membrane hydration level. The modeling domain was restricted to one honeycomb pore which was sufficient to obtain first fundamental understanding.

Later on, another CFD analysis was conducted by Berning and Tanaka [21], who used a non-isothermal, multiphase model based on CFX-4.4 (ANSYS Inc., Canonsburg, PA, USA) that included a prior developed membrane model [22]. The length of the channel section was 600 microns, and five holes were resolved in the numerical mesh, limited by the number of numerical blocks that could be used in that study. They surprisingly found that the pores in the metal GDL remained open, i.e., that no liquid water was penetrating and blocking the pores, despite the fact that the inlet relative humidity of the air was at 100%, and that liquid water was residing throughout the MPL. Among the other findings were a limiting current density higher than to 2 A/cm^2, and the fact that the polymer electrolyte membrane was predicted to be ideally hydrated, also owing to the fact that the predicted maximum temperature increase was only in the order of 1 °C because of the high thermal conductivity of the metal plates.

In earlier work, Berning et al. suggested that the pore-size distribution of CFP is a key parameter in the liquid water transport through the GDL [23]: A wider pore-size distribution can help keeping the pores open and allow for higher limiting current densities as was demonstrated by Zhang et al. [24]. The reasoning was that in the extreme case of a CFP with all identical pores, the water would obviously experience the same capillary pressure in all pores, and therefore the entire porous medium would become flooded at a certain threshold value for the water pressure. Therefore, it could be expected that the fuel cells with perforated metal GDL will be subjected to severe flooding under wet operating conditions. Separately, Owejan et al. [25] have found that the fuel cell performance for a CFP with a wider pore-size distribution like SGL21BC is better under wet operating conditions than for the Toray 060 paper which has a more regular structure with a narrow PSD, thus supporting the speculations by Berning et al. [23].

An ensuing research question of that work was, whether fuel cell operating conditions can be devised that might permit a constant relative humidity (RH) of 100% along the cathode flow field channel. Berning and Djilali [26] have pointed out, how the change in RH along the flow channel depends on the pressure drop along the flow channel and the change in molar composition: owing to the pressure drop alone the RH would decrease along the flow channel if the gas composition and temperature remain constant, as follows out of Equation (19) below. On the other hand, in a PEMFC, oxygen is consumed and water is being produced so that the composition of the gas changes along the flow channel,

causing the RH to rise. It is a frequent observation that towards the outlet of both anode and cathode side, channel flooding exists [25]. Such flooding can cause severe problems in a fuel cell stack with hundreds of cells as this can lead to maldistribution of the feed gases.

The current work follows up on the previous work by Berning and Tanaka [21]. The air enters the fuel cell at 100% RH, and it is the goal that the fuel cell operates in such a way that the cathode side flow channel might remain at 100% RH from inlet to outlet. To this end, we present a mathematical model that takes into account the pressure drop along the cathode flow channel in a straight channel design. In addition, the change in molar composition of the incoming air is calculated, assuming a constant current density. Thereby, the resulting stoichiometric flow ratio that might allow for fuel cell operation at constant RH is calculated as function of the current density. In a next step, the model is refined to also calculate the limiting current density that could be attained under such conditions. Finally, considerations concerning the fuel cell power density and the corresponding compressor power are made based on an assumed cell voltage at the maximum operating current density that is taken to be 80% of the limiting current density.

2. Model Description

Compared to the much more complex models that utilize the methods of CFD, the model presented here is fairly simple. The pressure drop along the flow channel leads to a decrease in RH of the cathode air, which is ideally compensated by the change in molar composition owing to the electrochemical reactions, and the central question is: At which stoichiometric flow ratio is the velocity such that the decrease in RH due to the pressure drop is exactly compensated by the change in molar composition?

2.1. Model Assumptions

The following assumptions are made:

- The air is an ideal gas.
- All product water exits the cell at the cathode side.
- The flow is laminar to calculate the pressure drop.
- The channel flow is perfectly mixed.
- The temperature is constant.
- Oxygen and hydrogen cross-over is negligible.
- The velocity is constant in each control volume.
- The current density is constant.
- The condensation of water when the RH exceeds 100% is neglected.
- Convective flow in the holes of the perforated plate and the MPL is neglected.

2.2. Model Equations

2.2.1. Variable Current Density

In the first version of this model, the current density was taken as an input parameter. In a refined version of the model, the limiting current density was added as an output parameter to avoid assuming an input current density. With knowlegde of the limiting current density, operating conditions at various lower current densities could be determined.

The geometry is shown in Figure 3 where W_{Ch} denotes the width of a single channel and W_L the land area width. The area of the membrane-electrode assembly that is supplied by a single channel is:

$$A_{Mem} = (W_{Ch} + W_L) \times L_{Ch} = (1 + \frac{W_L}{W_{Ch}}) \times W_{Ch} \times L_{Ch} = (1 + \theta_{LW}) \times W_{Ch} \times L_{Ch}, \quad (7)$$

where L_{Ch} is the channel length and θ_{LW} is the land-to-channel-width ratio. The cross-sectional area of a single channel is:

$$A_{Ch} = W_{Ch} \times H_{Ch}, \quad (8)$$

where H_{Ch} is the channel height. It can also be seen that the wetted perimeter is given by:

$$p_{wet} = 2 \times W_{Ch} + 2 \times H_{Ch}. \tag{9}$$

A central equation in this model is the Hagen-Poiseuille equation which relates the velocity and the pressure drop in a circular pipe flow. It is conveniently written in the following form:

$$\Delta P = 32\mu \frac{L_{Ch}}{D_h^2} \times u \tag{10}$$

where μ is the fluid viscosity which was automatically evaluated, and it is in the range of 2.0×10^{-5} kg m^{-1} s^{-1}, L_{Ch} is the channel length, u is the average velocity and D_h is the hydraulic diameter of the channel. The Hagen-Poiseuille equation was fundamentally derived for a circular pipe, and it requires the flow to be laminar. However, turbulent flow could be easily captured as well by applying appropriate friction factors. For a rectangular channel, the pipe diameter is replaced by the hydraulic diameter, according to:

$$D_h = 4 \times \frac{A_{Ch}}{p_{wet}}. \tag{11}$$

Here, A_{Ch} is the cross-sectional channel area and p_{wet} the wetted perimeter. The average velocity at the channel inlet is given by [8]:

$$u_{in} = \lambda \times \frac{i}{4F} \frac{1}{x_{O_2,in}} \frac{RT}{P_{in}} \frac{A_{Mem}}{A_{Ch}}, \tag{12}$$

where i is the area-based current density, $x_{O_2,in}$ is the molar oxygen fraction, P_{in} the inlet pressure, R is the universal gas constant (8.314 J/mol-K), T is the temperature in [K], and A_{Mem} the active area that is fed by one channel.

When applying the Hagen-Poiseuille equation, it becomes obvious that in case there is a substantial pressure drop in the down-the-channel direction, the velocity increases because of the density change, and this has to be taken into account. With knowledge of the inlet velocity, the mass flow rate at the inlet can be calculated via:

$$\dot{m}_{in} = u_{in} \rho A_{Ch} \tag{13}$$

where the mixture density ρ is calculated out of the local pressure and composition according to the ideal gas law.

$$\rho = \frac{PW}{RT}. \tag{14}$$

where P is the pressure in [Pa], W is the molecular mass of the mixture, R is the universal gas constant 8.3145 J/mol-K, and T is the temperature in [K]. The mixture molecular mass can be calculated out of the molar fractions according to:

$$W = \sum_i x_i W_i \tag{15}$$

The total mass flow at the inlet is the sum of the mass flow rate of oxygen, nitrogen and water vapor which can be calculated out of the corresponding molar flow rates. The molar flow rate of oxygen at the inlet is:

$$\dot{n}_{O_2,in} = \lambda \times \frac{I}{4F}, \tag{16}$$

and the corresponding molar nitrogen flow rate is:

$$\dot{n}_{N_2,in} = \lambda \times \frac{79}{21} \frac{I}{4F}. \tag{17}$$

The molar inlet flow of water vapor can be calculated as [27]:

$$\dot{n}_{H_2O,in} = \lambda \times \frac{x_{H_2O,in}}{1 - x_{H_2O,in}} \left(1 + \frac{79}{21}\right) \frac{I}{4F}. \tag{18}$$

The molar fraction of water vapor can be calculated out of the requirement that the inlet relative humidity is 100%. Employing Dalton's law, one obtains:

$$\phi_{in} = 1 = \frac{P_{H_2O,in}}{P_{sat}(T)} = x_{H_2O,in} \times \frac{P_{in}}{P_{sat}(T)} \Rightarrow x_{H_2O,in} = \frac{P_{sat}(T)}{P_{in}}, \tag{19}$$

where ϕ denotes the relative humidity. The saturation pressure can be calculated out of Antoine's equation:

$$\log_{10}(P_{sat}) = A - \frac{B}{C + T} \tag{20}$$

where the pressure is in [Bar] and the temperature in [K]. The coefficients for water in the temperature range of interest between 334 K and 363 K are A = 5.0768, B = 1659.793, and C = −45.854, respectively [28].

As the cathode air streams down the channel, oxygen is consumed and replaced by water according to a locally specified current density. In this study the current density was assumed to be constant. At the same time, there is a pressure drop in the down-the-channel direction which can not be neglected in these micro-channels investigated here, and this leads to a change in density and the velocity. Therefore, the channel length was discretised and split up into a number of sections with the length Δx, as shown in Figure 4.

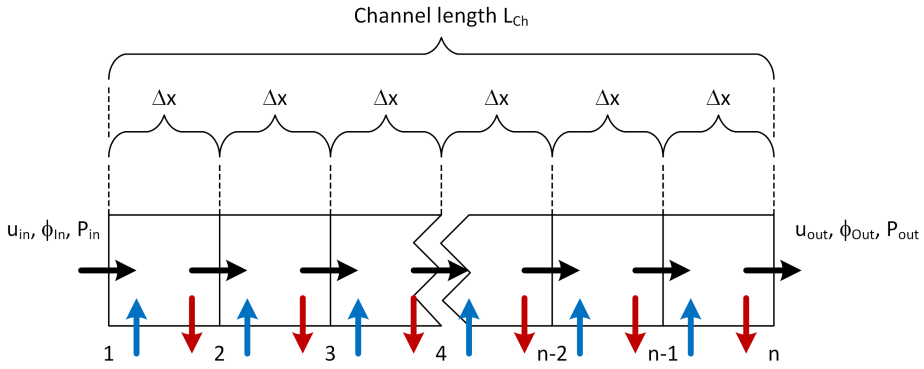

Figure 4. Flow channel discretization. Blue arrows indicate water vapour addition and red arrows oxygen subtraction.

The velocity at the interface between any two elements was calculated based on the updated mass flow rate and an updated pressure that fulfills the Hagen-Poiseuille equation for each control volume with length Δx. The mass flow rate of oxygen and water was updated based on the assumption of a uniform current density in each control volume (CV), and the velocity at the end of each CV was calculated as:

$$u_i = \frac{\dot{m}_i}{\rho_i A_{Ch}} \tag{21}$$

Regardless of the number of discretization volumes, this overall set of equations has as many equations as unknowns and is therefore a solvable problem.

In the first version of this model, the current density was employed as an input parameter. With this, the only unknown parameter was the stoichiometric flow ratio. The software that was used in these calculations was the Engineering Equation Solver (EES) V11.653 [29], a powerful tool to conduct any kind of engineering calculations provided the number of equations is equal to the number of unknowns. The solution method utilised

by EES is a modified version of the Newton-Raphson method for a nonlinear system of equations. It emerged, however, that EES was unable to find a solution for certain cases, e.g., when the temperature was set to 60 °C. Therefore, the model was also transported into MATLAB where a deterministic approach was successfully used.

2.2.2. Compressor Work

In a fuel cell system, the largest parasitic loss is usually the compressor work, calculated via:

$$\dot{W}_{comp,ideal} = \frac{\kappa}{\kappa - 1} \frac{RT}{W} \times \left[\left(\frac{P_2}{P_1} \right)^{\frac{\kappa-1}{\kappa}} - 1 \right] \times \dot{m} \tag{22}$$

Here, R is again the universal gas constant, and T is the gas temperature in [K]. For the calculations below, the average annual temperature in Denmark of 281.15 K was assumed. For the molecular weight W, we took the value for dry air of 28.84 g mol^{-1}. Finally, in the case of air, κ is 1.4. The mass flow rate $\dot{m}$ for every unit channel is calculated automatically by the model. However, as the air must pass the compressor before the humidifier, the mass of the dry air is used, neglecting the water in the ambient air. Through the compression, the air is also heated up to a value close to the fuel cell temperature.

The efficiency of a compressor depends strongly on its operating conditions. For simplicity, we assume a constant efficiency of η_s = 80%, so that the compressor work is calculated as:

$$\dot{W}_{comp} = \dot{W}_{comp,ideal} / \eta_s \tag{23}$$

2.2.3. Limiting Current Density

Because it was unknown, whether the prescribed current densities could be achieved, the limiting current density was added as a dependent parameter to the model. The theoretical limiting current density in a straight-channel flow field is determined out of the diffusion resistance between the bulk flow and the porous media, given as [5,30]:

$$i_l = 4F \frac{C_B}{\delta / D_{eff}} = 4F \frac{C_B}{R_{diff}} \tag{24}$$

where C_B is the molar concentration of oxygen in the bulk flow of the channel in [moles/m^3], δ is the diffusion length, and D_{eff} is the effective diffusion coefficient of oxygen in the humidified air through the porous metal plate and the porous MPL. The last two variables can be combined into a diffusion resistance R_{diff}.

To calculate the diffusion coefficient of oxygen through the humidified air, the binary diffusion coefficient between air and water vapour was employed [31]:

$$D_{air-H_2O} = 1.87 \times 10^{-10} \frac{T^{2.072}}{P_{atm}} \tag{25}$$

where D_{air-H_2O} is the binary diffusion coefficient in [m^2/s] and the pressure is given in [atm]. In order to calculate the effective diffusivity in the porous medium, this binary diffusion coefficient has to be corrected for the porosity ϵ and the tortuosity τ:

$$D_{eff} = D_{air-H_2O} \times \frac{\epsilon}{\tau} \tag{26}$$

For the MPL, the porosity was set to 0.75 and the tortuosity equal to 3. For the diffusion resistance inside the perforated plate, the porosity is calculated as:

$$\epsilon_{GDL} = \frac{\pi D_{hole}^2}{4\psi^2} \tag{27}$$

where ψ is the pitch, i.e., distance between two hole centres. The typical diameter of the holes ranges from 60–110 microns [18], and the land area between the holes is 50 microns, meaning the pitch ψ will be 110–160 microns. In the porous metal plates, the tortuosity τ is taken to be one. Thus, the total diffusion resistance is calculated as the sum of the resistance in the MPL and the GDL:

$$R_{tot} = R_{GDL} + R_{MPL} = \frac{\delta_{GDL}}{D_{eff,GDL}} + \frac{\delta_{MPL}}{D_{eff,MPL}} \tag{28}$$

where δ_{GDL} is the thickness of the GDL, while the diffusion length for the MPL was taken as half the land width. The limiting current density is then calculated in every node j as:

$$i_{L,j} = 4F \times \frac{C_{B,j}}{R_{tot}} \tag{29}$$

Finally, an average value is calculated, according to:

$$i_L = \frac{1}{n} \sum_{j=1}^{n} i_{L,j} \tag{30}$$

With this, the current density as an input parameter to the model has been eliminated, and the calculated stoichiometry is entirely a function of the operating conditions as well as the geometrical properties of the channels, the GDL and the MPL. It is understood that it is impossible to operate the cell at the limiting current density as the cell voltage would be by definition zero. However, important insight can be gained because it is desirable to operate these fuel cells at as high a current density as possible.

As was mentioned above, a weakness of this approach is that it neglects the resistance of oxygen in the catalyst layer themselves, i.e., the dissolution into the ionomer phase. Kudo et al. have shown that the single largest resistance to the oxygen transport is the dissolution into the ionomer phase and have proposed an agglomerate model to account for the various transport resistances [32,33].

2.3. Model Parameters

The parameter range investigated is listed in Table 1. The fuel cells in questions are micro fuel cells with a straight-channel flow field that are shorter than typical automotive ones, and it is the underlying idea to operate at high current densities.

Table 1. Overview of parameters and base case values.

Parameter	Symbol	Range [mm]	Base Case [mm]
Channel Length	L_{Ch}	50–150	100
Channel Height	H_{Ch}	0.15–0.30	0.20
Channel Width	W_{Ch}	0.15–0.30	0.20
Land Width	W_L	0.15–0.30	0.20

The temperature was varied between 60 °C and 80 °C, and the total pressure at the cathode outlet was fixed to 1 atm. In the first part of this study, the current density was left as adjustable parameter, and it was varied between 3 and 6 A/cm^2.

3. Model Results

3.1. Calculation of the Stoichiometric Flow Ratio

The first study investigated the possibility of operating a PEM fuel cell at constant inlet and outlet RH, where the cell temperature, the channel dimensions, and the current density were used as input parameters. The question in all these cases was: At which stoichiometric flow ratio will the decrease in RH due to the pressure drop be exactly balanced by the change in molar fractions such that the RH might stay constant?

By comparison to a model that is based on CFD, the current model is relatively coarse, but it gives an indication about the feasibility of using certain geometrical properties and operating conditions. Moreover, the calculations presented here can deliver the boundary conditions that could be used in a CFD model.

3.1.1. Effect of Mesh Size

The effect of the mesh size was investigated and described in reference [34], and it was shown that essentially 11 grid points are already sufficient to obtain a solution with reasonable accuracy, and there were no differences when the grid was step-wise refined from 21 cells to 51 cells. However, the calculations were only a matter of seconds, so that the results presented here were obtained with a grid that contained 51 cells.

3.1.2. Effect of Channel Length and Width

The effect of the channel width on the resulting stoichiometric flow ratio is shown in Figures 5 and 6. The effect of the channel width is similar to the effect of the channel height, previously described in reference [34], in that a wider channel leads to higher stoichiometric flow ratio such that the pressure drop effect along the channel is balanced by the effect of the change in molar composition.

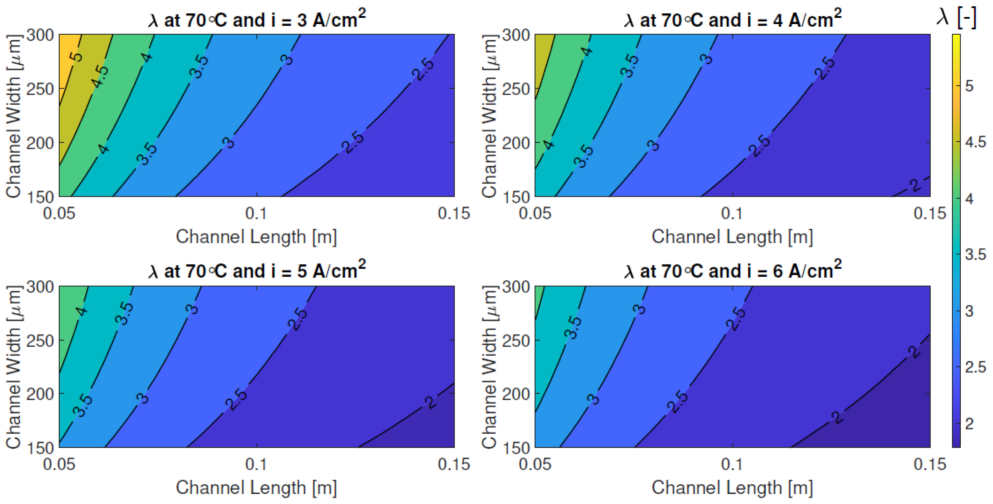

Figure 5. Calculated stoichiometry λ as function of channel length and width for different current densities at 70 °C.

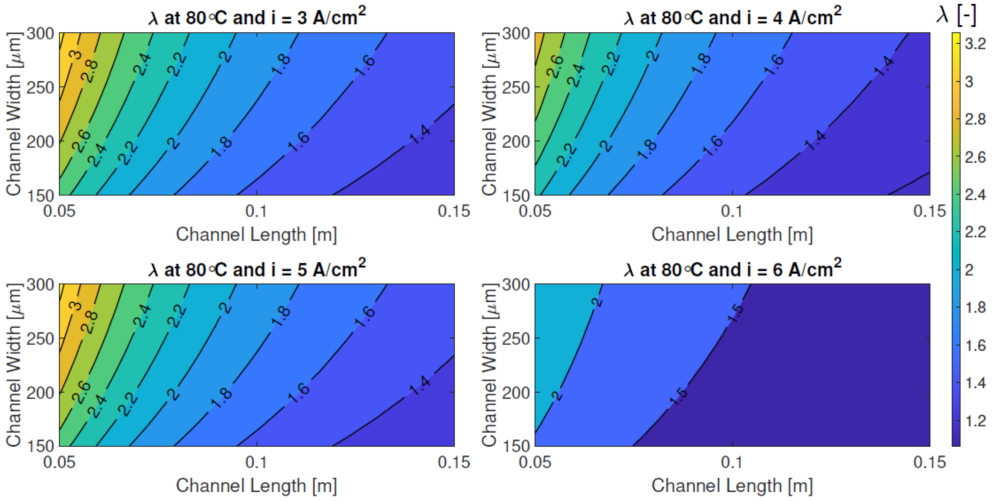

Figure 6. Calculated stoichiometry λ as function of channel length and width for different current densities at 80 °C.

The following trends were observed in detail:

- The lower cell temperature of 70 °C results in a higher stoichiometric flow ratio, the general range being between λ of 6 for the wide, short channel and under 2 for the narrow, long channel. With increasing current density, the required stoichiometry decreases.
- In the case of 80 °C, the same general trend are observed concerning the channel dimensions, but the required stoichiometries are lower, ranging from 3.5 to below 1.2.

Overall, the resulting values for the stoichiometry are lower than we originally expected. This, however, is encouraging as in the end it is the compressor work that is linearly proportional to the mass flow rate of air, and a lower stoichiometry leads to a reduced parasitic loss. This will be investigated in detail below.

3.1.3. Effect of Channel Length and Land-Width Ratio

Figures 7 and 8 show the calculated stoichiometries at two different temperatures for a varying land-width ratio.

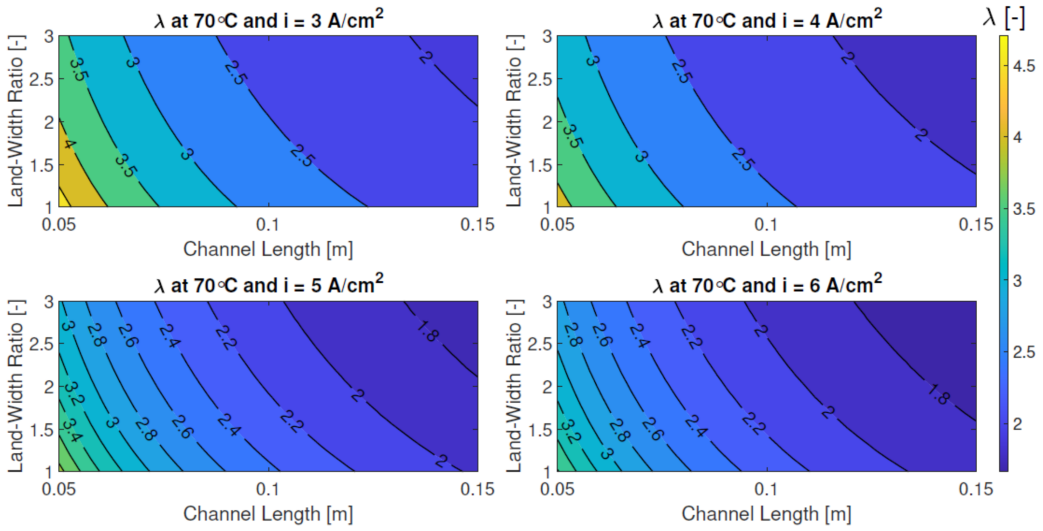

Figure 7. Calculated stoichiometry λ as function of channel length and land-width ratio θ_{LW} for different current densities at 70 °C.

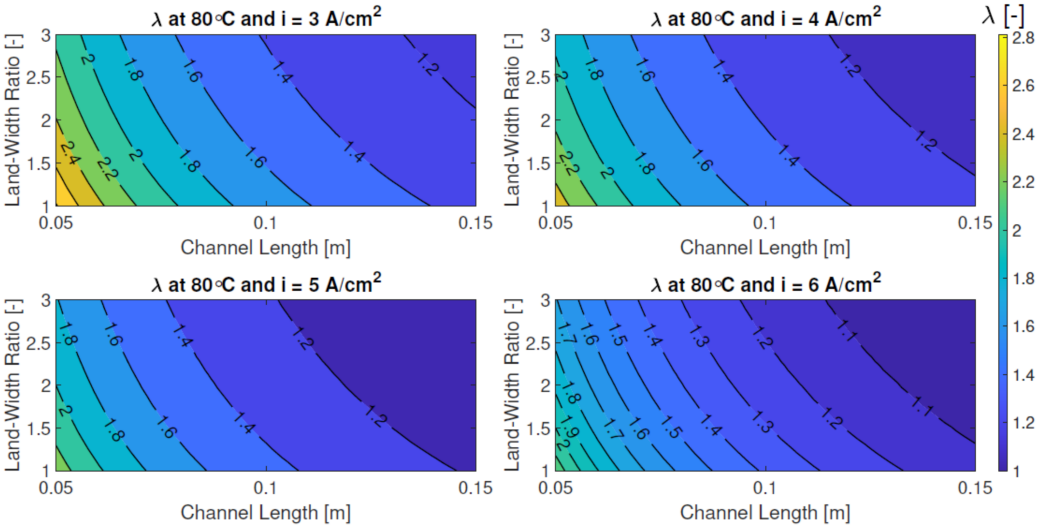

Figure 8. Calculated stoichiometry λ as function of channel length and land-width ratio θ_{LW} for different current densities at 80 °C.

The fundamental explanation for the observation that the resulting stoichiometric flow ratio is lower for a longer channel is that a longer channel automatically leads to a higher inlet velocity compared to a shorter channel, which also follows from Equation (12), and thus leading to higher pressure drop. A lower stoichiometry on the other hand means that the change in gas composition along the channel is more pronounced. Thereby, the effect of the strong reduction in RH due to the high velocity (high pressure drop) has to be balanced by a stronger change in gas composition, resulting in a lower stoichiometry for longer channels. The same argumentation can be made for the change in current density.

It can also be seen that here, an increase in the land-width ratio leads to a lower required stoichiometry. The reason for this is that every channel section now needs to supply a wider land width with oxygen, but the effect is surprisingly small. For example, Figure 8 shows for a current density of 6 A/cm^2 and a channel length of 5 cm, the resulting stoichiometry is $\lambda = 2.1$ at a land-width-ratio of one, and it decreases to $\lambda = 1.7$ for a land-width-ratio of 3. From this, it might be concluded that a higher land-width-ratio is generally beneficial, because in practice it would also lead to lower contact resistances, but a closer examination also reveals that in that case the RH in the middle of the channel exceeds the target value of 100% by far, and this would lead to channel condensation which we aim to avoid. This will be discussed next.

3.1.4. Comparison of the Channel RH Distribution

The model also allows for an optimization procedure, given a certain interval of parameters. In our case, we were interested in the best case and the worst case RH distribution along the channel length. In all cases, the inlet and outlet RH was set to 100%, but, as was mentioned above, it was observed that the RH increases to above 100% in the middle of the channel such that undesired channel condensation would occur.

Figure 9 summarizes the range of the RH distribution. Clearly, a shorter channel and low current density will lead to a more uniform RH distribution. In addition, the highest temperature, highest and widest channel, and lowest channel-to-land ratio lead to the highest RH uniformity while the opposite parameters lead to the worst case where the calculated theoretical RH can exceed 180%. However, the amount if liquid water produced would still be small because of the change in density between water vapor and liquid water.

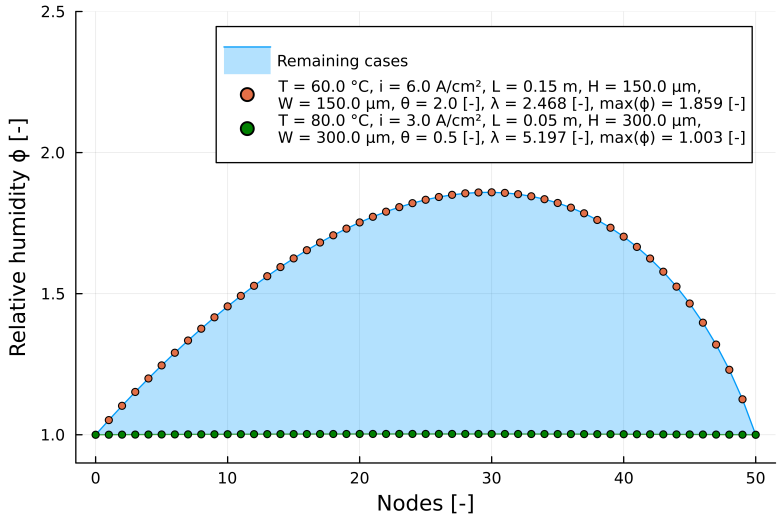

Figure 9. Comparison of best and worse case RH distribution

In general, a wider land area is preferable as it will lead to a lower contact resistance. On the other hand, the inlet RH can be drastically reduced in order to reduce the size of the humidifier. Thus, in the future it should be investigated, under which conditions the channel RH will remain below 100% when the inlet RH is decreased, while at the same time

the membrane is prevented from dehydration. Such questions can be investigated with a combination of the current one-dimensional model, and multi-dimensional CFD modeling.

The model developed so far gives no indication, whether it is in fact possible to operate a fuel cell at such low stoichiometries and high currents. Therefore, the model was refined and the limiting current density was added as a key parameter. However, the textbook definition of the limiting current density only accounts for the mass transport resistances between the gas flow channels and the cathode catalyst layer.

3.2. Calculation of the Limiting Current Density

In this section, modeling results will be presented with the enhanced model where the limiting current according to textbook definition was taken into account. Because it was found that the relative humidity exceeds 100% in the middle of the channel, the inlet RH was reduced to 95% in these cases while the outlet RH was fixed to 100% for all cases. Note that the model allows for an arbitrary specification of both desired inlet and outlet relative humidity.

The number of material parameters that play a role is now quite large. It was a goal to elucidate, what the maximum values for the limiting current density are reasonable. In the following, the shortest channel length of 50 mm was used, along with the deepest channels of 0.3 mm paired with the finest channel and land width of 0.15 mm, respectively.

Experience from using the built-in optimization tool in EES has shown that these values yield the highest limiting current densities. For the holes in the metal GDL, again the values for the lowest transport resistances here were chosen. All properties are listed in Table 2.

Table 2. Overview of parameters for the calculation of the limiting current density.

Parameter	Symbol	Value [mm]
Channel length	L_{Ch}	50
Channel height	H_{Ch}	0.300
Channel width	W_{Ch}	0.150
Land width	W_{La}	0.150
Hole diameter	D_{hole}	0.110
Hole pitch	ψ	0.160
GDL thickness	δ_{GDL}	0.050
MPL thickness	δ_{MPL}	0.075

Figure 10 shows the resulting local limiting current density and the local RH distribution for three different temperatures. It is noted that the limiting current densities are surprisingly high, especially in the beginning of the channels where they range from 15–19 A/cm^2, depending on the temperature, and where the lowest temperature yields the highest value.

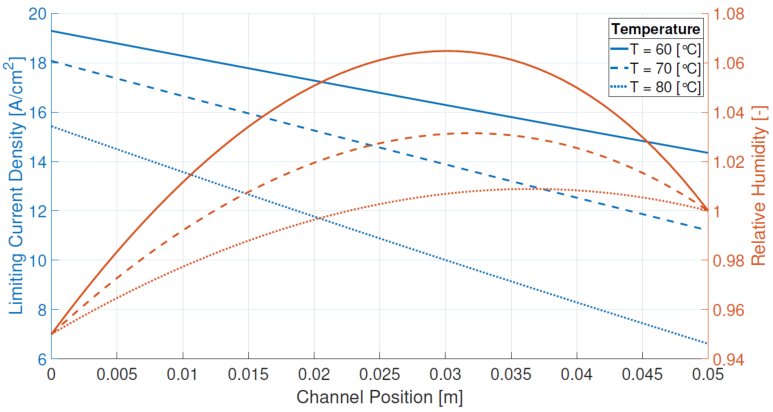

Figure 10. Calculated limiting current density (left axis) and relative humidity (right axis) distribution.

This results out of the fact that at the lowest temperature, the gas phase contains less water vapour and consequently a higher volume fraction of oxygen, and it is only the concentration of the oxygen that is considered for the calculation of the limiting current density. The combined thickness of the GDL and MPL is just 125 microns, and thus considerably less than typical materials [19].

Moreover, compared to standard CFP, the metal GDL has a lower porosity in the order of 35–40%, but an assumed tortuosity of unity, and the combination of both makes their diffusion resistance smaller. Another reason for the observed high limiting currents is the high inlet pressure which leads to a high oxygen concentration. Even the short channels of 50 mm length yield a pressure drop of 20–50 kPa over the length of the channel.

As was explained above, for the calculation of the overall limiting current density, the average values of the local ones were taken into account. It can be expected that when the fuel cell operates in a nearly isothermal mode as was observed when using the metal GDL [21], the current density is highest at the cathode inlet where the oxygen concentration is also highest.

The current proposed method of operating the fuel cell at constant (or controlled) relative humidity necessitates high pressure drops in the down-the-channel direction to accommodate the product water. An obvious advantage is that there will be no channel flooding, which has been the subject of extensive research efforts [25]. In order to judge, whether this method of fuel cell operation is generally preferred, the added mass flow rates and pressure drops that lead to a higher compression power need to be factored in.

Kudo et al. [32,33] have determined the additional oxygen resistance inside the polymer electrolyte, and found it to be substantial. Therefore, the limiting current densities according to the textbook definitions are a mere indication of how much oxygen can be transported towards the CCL, and in any way it is obvious that the fuel cell can not be operated at this limiting current as the cell voltage would be zero by definition.

3.3. Calculation of the Fuel Cell Power and Compressor Work

All considerations so far have been useful indications as to how the operating conditions of a PEMFC might be tuned, but in the end it is the performance of the fuel cell system that has to be optimized. It is well known that the compressor that supplies the air is a large parasitic loss in the fuel cell system, and high oxygen stoichiometries in conjunction with high pressure drops will lead to high parasitic losses [4].

To calculate the fuel cell power density in conjunction with the compressor work for the mass streams of air, the fuel cell voltage has to be taken into account. For simplicity, it is taken here to be 0.5 V. For the calculations of the compressor power, a constant compressor efficiency of 80% was assumed. In reality, compressor performance charts are complex, and the pairing of the compressor and the fuel cell stack is of great importance.

In this section, the theoretical net power of a fuel cell stack operated at an RH of 100% at both cathode inlet and outlet is calculated. Other input parameters are the channel geometry and the hole size and distribution of the porous metal GDL which have a strong influence on the limiting current density. While the channel geometry are the base case values as given in Table 1, the holes in the metal GDL were taken to be 100 microns in diameter with a pitch of 150 microns, thus a spacing of 50 microns. The thickness of the metal GDL was 50 microns which is in a similar range as the one made by Hussein et al. [18]. In the calculations of the limiting current density, the thickness of the metal GDL is of great importance. For example, when the GDL thickness is 50 microns, the limiting current density in case of a 50 mm long channel at 65 °C is 13.07 A/cm^2, while it drops to 10.35 A/cm^2 when the thickness is 100 microns and 8.57 A/cm^2 when the thickness is 150 microns.

With these input parameters, the limiting current density can be calculated by the model. However, as it is impossible to operate a fuel cell at the limiting current density, it is assumed that the maximum operating current density is 80% of the limiting current, and

it is denoted as i_{80}. As mentioned above, it is then assumed that the operating voltage is U_{cell} = 0.5 V at this current. The net power density is calculated out of:

$$\dot{w}_{net} = U_{cell} i_{80} - \dot{W}_{comp} / A_{MEA} \quad (31)$$

Clearly, this assumption has to be revised with better understanding of the fuel cell polarization curve. The calculated power density is taken to be 80% of the limiting current density multiplied with the assumed cell voltage. All other parameters are directly calculated by the model, using only the geometric parameters and the requirement that both inlet and outlet relative humidity are at 100% as input parameters.

Some of the detailed output parameters of our model are summarized in Tables 3–8 for the three different channel lengths and four different temperatures. In Tables 3–5, the following observations are made:

- The limiting current densities which are the averaged values over the length of the cell are surprisingly high, ranging from 8.38 A/cm^2 to 13.52 A/cm^2. These values are calculated out of the oxygen concentration inside the flow channels, and therefore they vary with pressure drop and compositions. A higher temperature means that there is a higher concentration of water vapour in the mixture to yield a relative humidity of 100%, and therefore the limiting current density decreases with increasing temperature. The dependency between the limiting current density and the channel length is weak, and this suggests that the longer channels might be preferable. For large-scale applications such as automotive, it is difficult to see how channels in the order of 50 mm could be practical.
- The assumed operating current i_{80} is 80% of the limiting current, and it therefore shows the same behaviour as the first column. The power density curve of a fuel cell typically peaks at 80% of the limiting current, as was also suggested in Figure 2. In practice, fuel cell manufacturers can adjust the amount of catalyst such that the power density shows the desired behavior.
- The stoichiometric flow ratio is the value that corresponds to the operating current density i_{80}. As was noticed before, the calculated values are surprisingly low, which is due to the fact that the channel height and width are small, causing a high pressure drop. In fact, for the current cases, it is the stoichiometry that is limiting the length of the channels as clearly it is not physical to go to values below 1. Already a case of $\lambda = 1.11$ as was calculated for a channel length of 150 mm and a temperature of 80 °C seems not plausible. In any case, experiments are required. From the model alone we can deduce that the stoichiometry is a key output parameter because it determines the maximum channel length. It can also be expected that for a fuel cell operating temperature of 85 °C, the channel length is limited to around 100 mm. However, findings from the first part were that a higher channel results in higher stoichiometries, and a quick test revealed that when the channel height is increased to 300 microns, i_{80} becomes 6.85 A/cm^2 instead of 6.70 A/cm^2, and the corresponding stoichiometry is 1.32 instead of 1.11.
- The next column lists the pressure drop. In conjunction with the total mass flow rate, this is a key parameter for the sizing of the compressor. For typical automotive applications, turbocompressors deliver a pressure in the range of 2–2.5 bar, hence up to 250 kPa. In the current application, the pressure drop is lower but for a fuel cell system it is quite high. It must be remembered that this high pressure drop is required to accommodate the product water and keep the relative humidity ideally constant from inlet to outlet. The required pressure drop decreases with temperature because the total mass flow rate also decreases, and it scales almost linearly with the channel length.
- The Reynolds number have been monitored because it is important to stay in the laminar flow regimes. Generally, for straight channel flow, turbulence will set in at Re number of 2000, and laminar flow is a key assumption when using the Hagen-

Poiseuille equation for the calculation of the pressure drop as was done here. The benchmark value of 2000 is an approximation and frequently observed in experiments, but in the gas flow channels here, the flow is disturbed and one oxygen molecule is replaced with two water molecules, and therefore we can expect the onset of turbulence at a lower Re-number.

- The final column lists the mass flow rate. As mentioned above, in conjunction with the pressure drop, this parameter is key for the sizing of the compressor. Interestingly, the mass flow rate does not scale linearly with the channel length. Together with the observation that the limiting current density shows only a weak dependency on the channel length, this might also be an argument to use longer channels. Thus, a given compressor can serve a larger and more powerful fuel cell stack. This will be shown in more detail below.

Overall, the most important observation is probably that the mass flow rates would suggest to use as long a channel as possible, but the ultimate length of the channel is limited by the stoichiometric flow ratio and the operating temperature. The channel length has only a weak effect on the calculated limiting current density.

Table 3. Key results I as function of temperature for a channel length of 50 mm.

T_{cell} [°C]	i_l [A/cm^2]	i_{80} [A/cm^2]	λ [-]	ΔP [kPa]	Re [-]	$\dot{m}$ [mg/s]
65	13.07	10.45	3.75	50.35	792	3.13
70	12.03	9.62	3.07	42.32	623	2.47
75	10.72	8.57	2.50	34.85	483	1.90
80	9.07	7.26	2.02	27.78	367	1.42

Table 4. Key results I as function of temperature for a channel length of 100 mm.

T_{cell} [°C]	i_l [A/cm^2]	i_{80} [A/cm^2]	λ [-]	ΔP [kPa]	Re [-]	$\dot{m}$ [mg/s]
65	13.19	10.56	2.54	107.9	1048	4.15
70	11.96	9.57	2.06	89.8	794	3.14
75	10.44	8.35	1.66	72.9	591	2.32
80	8.57	6.86	1.34	57.0	427	1.66

Table 5. Key results I as function of temperature for a channel length of 150 mm.

T_{cell} [°C]	i_l [A/cm^2]	i_{80} [A/cm^2]	λ [-]	ΔP [kPa]	Re [-]	$\dot{m}$ [mg/s]
65	13.52	10.81	2.15	170.9	1337	5.29
70	12.14	9.71	1.73	141.6	987	3.91
75	10.44	8.35	1.38	114.2	712	2.80
80	8.38	6.70	1.11	88.0	494	1.92

Next, Tables 6–8 list information concerning the power generated by the fuel cell system. While this is certainly a key parameter, the considerations suffer from the assumption that the cell voltage is 0.5 V at the operating current i_{80}. Therefore, these calculations are merely of exemplary nature and have to be revised with a better understanding of the polarization curve. The following key results are summarized:

- The first columns list the specific power delivered by the fuel cell, and it is merely the product of the operating, maximum current density i_{80} and the cell voltage. Clearly, the lower operating temperatures yield the highest power, simply because the limiting current densities were higher. The drop off in power becomes steeper at the higher temperatures; while the relative drop-off was 10% between 65 °C and 70 °C it is 20% between 75 °C and 80 °C.

- The specific compressor power calculated out of the mass flow rate and the pressure drop according to Equation (23). This value also decreases with increasing temperature, owing to the fact that both pressure drop and mass flow rates decrease.
- The percentage of the compressor power compared to the fuel cell power is slightly higher than the values calculated by Berning et al. [4]. Given all other uncertainties, it should probably be kept around 5%, but for automotive applications, the size and cost of the compressor plays an important role as well.
- The next columns lists the net power density, i.e., the fuel cell generated power density minus the specific compressor power, and this should be the most important column overall. In the current analysis, the values are biased towards the lower temperatures because of the assumption of a constant cell voltage at the given, high, operating currents. Net power densities in the region of 4 W/cm^2 would be very high by current standards, and such high value also results out of the high operating current densities. At a temperature of 80 °C, the assumed cell voltage of 0.5 V may not be too optimistic. When considering the role of the channel length, this result would be a strong argument for the shorter channels, but it must be kept in mind that the mass flow rate of air did not scale linearly with the channel length.

Table 6. Key results II as function of temperature for a channel length of 50 mm.

T_{cell} [°C]	$\dot{w}_{cell}$ [W/cm^2]	$\dot{w}_{comp}$ [W/cm^2]	$\dot{w}_{comp}/\dot{w}_{cell}$ [%]	$\dot{w}_{net}$ [W/cm^2]	$\dot{W}_{abs}$ [W]	E_m [J/g]
65	5.23	0.601	11.5	4.63	0.925	296
70	4.81	0.389	8.08	4.41	0.885	358
75	4.29	0.237	5.53	4.05	0.810	426
80	3.63	0.132	3.60	3.50	0.699	492

Table 7. Key results II as function of temperature for a channel length of 100 mm.

T_{cell} [°C]	$\dot{w}_{cell}$ [W/cm^2]	$\dot{w}_{comp}$ [W/cm^2]	$\dot{w}_{comp}/\dot{w}_{cell}$ [%]	$\dot{w}_{net}$ [W/cm^2]	$\dot{W}_{abs}$ [W]	E_m [J/g]
65	5.28	0.776	14.7	4.50	1.80	434
70	4.79	0.491	10.3	4.29	1.72	547
75	4.17	0.292	6.99	3.88	1.55	669
80	3.43	0.157	4.58	3.27	1.31	789

Table 8. Key results II as function of temperature for a channel length of 150 mm.

T_{cell} [°C]	$\dot{w}_{cell}$ [W/cm^2]	$\dot{w}_{comp}$ [W/cm^2]	$\dot{w}_{comp}/\dot{w}_{cell}$ [%]	$\dot{w}_{net}$ [W/cm^2]	$\dot{W}_{abs}$ [W]	E_m [J/g]
65	5.41	0.955	17.7	4.45	2.67	505
70	4.86	0.598	12.3	4.26	2.55	653
75	4.18	0.349	8.36	3.83	2.30	820
80	3.35	0.183	5.46	3.17	1.90	990

- The total power per channel $\dot{W}_{abs}$ is listed in the next column. It is the net specific power density multiplied with the active area. Therefore, the longer channels deliver more power per channel than the shorter ones. Important is the combination of a suitable compressor and the fuel cell stack with sufficient power supply. For example, the compressor by Bosch that delivers around 250 g/s of air in the 20 kW power class would be suitable to power a stack of the size 250 g/s/1.92 mg/s × 1.90 W ≈ 250 kW for the long channels at 80 °C, but only a stack of the size 250 g/s/1.42 mg/s × 0.699 W ≈ 125 kW with shorter channels, assuming it is suitable to deliver at the required pressure. In the first case, the total number of channels would be 130,000. Taking the number of plates in an automotive fuel cell stack to be 260, we would need 500 parallel

channels per plate, and taking a channel and land width in the order of 0.5 mm, the stack would be 250 mm wide. In the latter case, the same considerations would lead to a stack of the same height, a width of 340 mm and 50 mm long channels that delivers half the power owing to the limitations of the compressor.

- The last columns was introduced to accommodate for the fact that the longer channels require a lower amount of mass flow compared to shorter channels, and it was calculated out of the power per channel divided by the mass flow rate per channel. Here, the highest temperature and the longest channel yield the highest value. However, how practical this particular property is remains to be seen.

4. Conclusions

A one-dimensional model of the cathode flow channel in a PEMFC has been developed to investigate, under which conditions such fuel cells may operate at a constant relative humidity. To this end, the pressure drop along the flow channel was calculated with the Hagen-Poiseuille equation, and the change in the molar gas composition was calculated assuming a uniform current density. Moreover, it was assumed that porous metal plates with uniform hole distribution were used as porous transport layers instead of the more common carbon fiber papers for improved waste heat management. First input parameters of the model were the current density and temperature, both of which were varied, and the back pressure which was taken to be ambient in the current study. Other input parameters were the channel dimensions and physical properties of the metal GDL and the MPL. Thus, all geometrical parameters are taken into consideration, and therefore this model can be used for dimensioning the cathode flow channels.

The first key output parameter was the stoichiometric flow ratio that would allow possible constant RH operation. This parameter, along with the calculated pressure drop, could be used as a boundary condition in a detailed CFD analysis. The calculated stoichiometry depends on all channel dimensions, and the values are generally low and depend on the current density.

In order to eliminate the current density as input parameter, the model was then refined to calculate the limiting current density which depends on the oxygen concentration in the flow channel and the diffusion resistance between the channel and the cathode catalyst layer. The calculated limiting current densities turned out to be surprisingly high which was caused by the high pressure drop of these fuel cells which lead to a high oxygen concentration at the inlet region, and the generally lower diffusion resistances of the thin metal GDL. Simplified calculations of the expected cell power density yielded values in the region of 4 A/cm^2, afforded by the high current density and an assumed cell voltage of 0.5 V. The compressor work should not exceed 5% of the fuel cell power, and this suggests operating temperatures in the region of 80 °C.

Recently, our research group has published a CFD analysis that verifies the principle findings of the here presented study in that such high current densities appear feasible [35]. It was verified that the unprecedented high pressure drop allows the air to expand inside the cathode flow field channels and thus make room for the product water with the result that channel flooding is prevented. In the future, it could furthermore be explored, how the pores of the metal GDL could be distributed such that a desired adjustment of the effective diffusion coefficient from inlet to outlet could be obtained [36].

Author Contributions: Conceptualization, T.B.; methodology, N.M.B., R.D.S., M.J., K.K. and T.B.; software, N.M.B., R.D.S., M.J. and K.K.; formal analysis, N.M.B., R.D.S., M.J., K.K. and T.B.; investigation, N.M.B., R.D.S., M.J. and K.K.; data curation, N.M.B., R.D.S., M.J. and K.K.; writing—original draft preparation, T.B.; writing—review and editing, N.M.B., R.D.S. and T.B.; visualization, N.M.B. and R.D.S. All authors have read and agreed to the published version of the manuscript.

Funding: This work received no funding.

Data Availability Statement: The raw data supporting the conclusions of this article will be made available by the authors on request.

Acknowledgments: This work was in part conducted as a 6th semester Bachelors project at AAU Energy.

Conflicts of Interest: The authors declare no conflict of interest.

References

1. Ballard Power Systems. Ballard Stack Key Parameters. Available online: https://www.ballard.com/fuel-cell-solutions/fuel-cell-power-products/fuel-cell-stack (accessed on 30 May 2024).
2. Berning, T. Three-Dimensional Computational Analysis of Transport Phenomena in a PEM Fuel Cell. Ph.D. Thesis, University of Victoria, Victoria, BC, Canada, 2002.
3. Barbir, F.; Braun, J.; Neutzler, J. Effect of Collector Plate Resistance on Fuel Cell Stack Performance. *ECS Proc. Vol.* **1998**, *1998*, 400. [CrossRef]
4. Berning, T.; Odgaard, M.; Kær, S.K. A study of multi-phase flow through the cathode side of an interdigitated flow field using a multi-fluid model. *J. Power Sources* **2010**, *195*, 4842–4852. [CrossRef]
5. Barbir, F. *PEM Fuel Cells*, 2nd ed.; Elsevier: Amsterdam, The Netherlands, 2012.
6. Zhang, G.; Guo, L.; Ma, L.; Liu, H. Simultaneous measurement of current and temperature distributions in a proton exchange membrane fuel cell. *J. Power Sources* **2010**, *195*, 3597–3604. [CrossRef]
7. Inman, K.; Wang, X.; Sangeorzan, B. Design of an optical thermal sensor for proton exchange membrane fuel cell temperature measurement using phosphor thermometry. *J. Power Sources* **2010**, *195*, 4753–4757. [CrossRef]
8. Berning, T.; Lu, D.; Djilali, N. Three-dimensional computational analysis of transport phenomena in a PEM fuel cell. *J. Power Sources* **2002**, *106*, 284–294. [CrossRef]
9. Wang, C.Y. Fundamental Models for Fuel Cell Engineering. *Chem. Rev.* **2004**, *104*, 4727–4766. [CrossRef] [PubMed]
10. Berning, T.; Kær, S. Low stoichiometry operation of a proton exchange membrane fuel cell employing the interdigitated flow field—A modeling study. *Int. J. Hydrogen Energy* **2012**, *37*, 8477–8489. [CrossRef]
11. Rieke, P.C.; Vanderborgh, N.E. Temperature dependence of water content and proton conductivity in polyperfluorosulfonic acid membranes. *J. Membr. Sci.* **1987**, *32*, 313–328. [CrossRef]
12. Avramov, S.; Lefterova, E.; Penchev, H.; Sinigersky, V.; Slavcheva, E. Comparative study on the proton conductivity of perfluorosulfonic and polybenzimidazole based polymer electrolyte membranes. *Bulg. Chem. Commun.* **2016**, *48*, 43–50.
13. Karimi, G.; Li, X.; Teertstra, P. Measurement of through-plane effective thermal conductivity and contact resistance in PEM fuel cell diffusion media. *Electrochim. Acta* **2010**, *55*, 1619–1625. [CrossRef]
14. Burheim, O.S.; Pharoah, J.G.; Lampert, H.; Vie, P.J.S.; Kjelstrup, S. Through-Plane Thermal Conductivity of PEMFC Porous Transport Layers. *J. Fuel Cell Sci. Technol.* **2010**, *8*, 021013, [CrossRef]
15. Yablecki, J.; Bazylak, A. Determining the effective thermal conductivity of compressed PEMFC GDLs through thermal resistance modelling. *J. Power Sources* **2012**, *217*, 470–478. [CrossRef]
16. Csoklich, C.; Sabharwal, M.; Schmidt, T.J.; Büchi, F.N. Does the thermal conductivity of gas diffusion layer matter in polymer electrolyte fuel cells? *J. Power Sources* **2022**, *540*, 231539. [CrossRef]
17. Fernihough, O.; Ismail, M.S.; El-kharouf, A. Intermediate Temperature PEFC's with Nafion® 211 Membrane Electrolytes: An Experimental and Numerical Study. *Membranes* **2022**, *12*, 430. [CrossRef] [PubMed]
18. Hussain, N.; Van Steen, E.; Tanaka, S.; Levecque, P. Metal based gas diffusion layers for enhanced fuel cell performance at high current densities. *J. Power Sources* **2017**, *337*, 18–24. [CrossRef]
19. Gostick, J.T.; Fowler, M.W.; Ioannidis, M.A.; Pritzker, M.D.; Volfkovich, Y.; Sakars, A. Capillary pressure and hydrophilic porosity in gas diffusion layers for polymer electrolyte fuel cells. *J. Power Sources* **2006**, *156*, 375–387. [CrossRef]
20. Tanaka, S.; Malan, A.G. Investigating design parameters of a perforated metal gas diffusion layer in a polymer electrolyte membrane fuel cell. *J. Power Sources* **2019**, *413*, 198–208. [CrossRef]
21. Berning, T.; Tanaka, S. A Study of Multiphase Flow and Heat Transfer in Proton Exchange Membrane Fuel Cells With Perforated Metal Gas Diffusion Layers. In *Fluids Engineering Division Summer Meeting*; Volume 2: Computational Fluid Dynamics; American Society of Mechanical Engineers: Houston, TX, USA, 2019. [CrossRef]
22. Berning, T.; Odgaard, M.; Kær, S. Water balance simulations of a polymer-electrolyte membrane fuel cell using a two-fluid model. *J. Power Sources* **2011**, *196*, 6305–6317. [CrossRef]
23. Berning, T.; Odgaard, M.; Kær, S.K. A Computational Analysis of Multiphase Flow Through PEMFC Cathode Porous Media Using the Multifluid Approach. *J. Electrochem. Soc.* **2009**, *156*, B1301. [CrossRef]
24. Zhang, J.; Kramer, D.; Shimoi, R.; Ono, Y.; Lehmann, E.; Wokaun, A.; Shinohara, K.; Scherer, G.G. In situ diagnostic of two-phase flow phenomena in polymer electrolyte fuel cells by neutron imaging: Part B. Material variations. *Electrochim. Acta* **2006**, *51*, 2715–2727. [CrossRef]
25. Owejan, J.; Trabold, T.; Jacobson, D.; Arif, M.; Kandlikar, S. Effects of flow field and diffusion layer properties on water accumulation in a PEM fuel cell. *Int. J. Hydrogen Energy* **2007**, *32*, 4489–4502. [CrossRef]
26. Berning, T.; Djilali, N. A 3D, Multiphase, Multicomponent Model of the Cathode and Anode of a PEM Fuel Cell. *J. Electrochem. Soc.* **2003**, *150*, A1589. [CrossRef]

27. Berning, T. The dew point temperature as a criterion for optimizing the operating conditions of proton exchange membrane fuel cells. *Int. J. Hydrogen Energy* **2012**, *37*, 10265–10275. [CrossRef]
28. National Institute of Standards and Technology. Antoine Equation Parameters for Water. 2024. Available online: https://webbook.nist.gov/cgi/cbook.cgi?ID=C7732185&Mask=4&Type=ANTOINE&Plot=on#ANTOINE (accessed on 1 August 2024).
29. Klein, S.A. EES—Engineering Equation Solver. Version 11.653, F-Chart Software. Available online: https://fchartsoftware.com (accessed on 1 August 2023).
30. O'Hayre, R.; PhD, S.W.C.; Colella, W.; Prinz, F.B. Chapter 5: Fuel Cell Mass Transport. In *Fuel Cell Fundamentals*; John Wiley & Sons, Ltd.: Hoboken, NJ, USA, 2016; Chapter 5, pp. 167–202. [CrossRef]
31. Marrero, T.R.; Mason, E.A. Gaseous Diffusion Coefficients. *J. Phys. Chem. Ref. Data* **1972**, *1*, 3–118. [CrossRef]
32. Kudo, K.; Suzuki, T.; Morimoto, Y. Analysis of Oxygen Dissolution Rate from Gas Phase into Nafion Surface and Development of an Agglomerate Model. *ECS Trans.* **2010**, *33*, 1495. [CrossRef]
33. Kudo, K.; Morimoto, Y. Analysis of Oxygen Transport Resistance of Nafion Thin Film on Pt Electrode. *ECS Trans.* **2013**, *50*, 1487. [CrossRef]
34. Bielefeld, N.M.; Sørensen, R.D.; Jørgensen, M.; Kure, K.S.; Berning, T. Operating Proton Exchange Membrane Fuel Cells at a Constant Relative Humidity. *ECS Trans.* **2022**, *108*, 3. [CrossRef]
35. Liu, W.; Olesen, A.C.; Liso, V.; Berning, T. High Current Density Operation of a Proton Exchange Membrane Fuel Cell with Varying Inlet Relative Humidity—A Modeling Study. *Energies* **2024**, *17*, 4077. [CrossRef]
36. Berning, T.; Wieser, C.; Chuang, P.Y.A.; Trabold, T.A. Method for Optimizing Diffusion Media with Spatially Varying Mass Transport Resistance. U.S. Patent 7,829,230, 9 November 2010.